Published in final edited form as:
Neuroimage. 2010 January 15; 49(2): 1416–1431. doi:10.1016/j.neuroimage.2009.09.044.

Bimodal Modulation and Continuous Stimulation in Optical Imaging to Map Direction Selectivity

M. P. Vanni[1,2], **J. Provost**[3,*], **C. Casanova**[1], and **F. Lesage**[3]

[1] Laboratoire des Neurosciences de la Vision, École d'optométrie, Université de Montréal, Montréal, Québec, Canada

[2] Faculté de Médecine, Université de Montréal, Montréal, Québec, Canada

[3] Département de génie électrique et Institut de génie biomédical, École Polytechnique de Montréal, Montréal, Québec, Canada

Abstract

In the visual system, neurons with similar functional properties such as orientation and direction selectivity are clustered together to form modules. Optical imaging recordings in combination with episodic paradigms have been previously used to estimate direction selectivity, a fundamental property of visual neurons. The major drawback of the episodic approach is that the extraction of the signal from various forms of physiological noise is difficult, leading to a poor estimation of direction. Recent work, based on periodic stimulation and Fourier decomposition improved the extraction of periodic stimulus responses from noise and thus, reduced the recording time considerably. Given the success of this new paradigm in mapping orientation, the present study evaluated its reliability to measure direction selectivity in the visual cortex of anesthetised cats. Here, a model that exploits the harmonics of the Fourier decomposition is proposed where the first harmonic is related to direction responses, and the second to orientation. As expected, the first harmonic was absent when a static stimulus was presented. Contrarily, the first harmonic was present when moving stimuli were presented and the amplitude was greater with random dots kinematograms than with drifting gratings. The phase of the first harmonic showed a good agreement with direction preference measured by episodic paradigm. The ratio of the first/the second harmonic amplitude, related to a direction index, was weaker in fracture. It was also weaker in areas of the ventral pathway (areas 17 and 21a) where direction selectivity is known to be reduced. These results indicate that a periodic paradigm can be easily used to measure specific parameters in optical signals, particularly in situations when short acquisition periods are needed.

Keywords

area 17; area 18; cat; Fourier; intrinsic signals; orientation selectivity; spatial frequency; motion; visual cortex; cortical map

Corresponding Author: Dr. Christian Casanova, Laboratoire des Neurosciences de la Vision, École d'optométrie, Université de Montréal, CP 6128, succ. Centre-ville, Montréal, Québec, Canada, H3C 3J7, Tel. (514) 343-2407, Fax. (514) 343-2382, christian.casanova@umontreal.ca, Web: http://www.opto.umontreal.ca/neurosciences/.
*Present address: Biomedical Engineering Department, Columbia University, New York, NY, USA.

INTRODUCTION

It is well established that, in sensory systems, neurons with similar functional properties are clustered together to form modules. On the surface of the cortex, the selectivity of neurons changes gradually, forming cortical maps, such in the case of orientation in the primary visual cortex of cats and primates (Bonhoeffer and Grinvald, 1991; Frostig et al., 1990; Grinvald et al., 1986). In these maps, orientation selectivity of neurons changes steadily, forming domains that converge in singularities called “pinwheels”. A separate clustering of direction selectivity associated with orientation maps has also been revealed (Swindale et al., 1987; Tolhurst et al., 1981). This arrangement ultimately leads to the formation of direction selectivity maps. Along this spatial functional organization, iso-orientation columns are divided into columns of preference for opposite directions, orthogonal to the preferred orientation (Henry et al., 1974; Kim et al., 1999; Kisvarday et al., 2001; Ribot et al., 2008; Shmuel and Grinvald, 1996; Swindale et al., 2003).

The organisation of direction selectivity was previously investigated by optical imaging of intrinsic signals (Kim et al., 1999; Kisvarday et al., 2001; Ribot et al., 2008; Shmuel and Grinvald, 1996; Swindale et al., 2003). In the first complete study (Shmuel and Grinvald, 1996), direction selectivity was calculated by the “vector sum”, a method generally used to compute orientation selectivity (Bonhoeffer and Grinvald, 1991, 1996; Grinvald et al., 1986; Kisvarday et al., 2001; Shmuel and Grinvald, 1996; Swindale, 1998). This approach is not ideal, particularly in regions of low selectivity because, in contrast to orientation, direction tuning is bimodal (Kisvarday et al., 2001; Swindale et al., 2003). Thus, when responses of opposite directions are close and the noise contribution significant, the vector sum does not provide a good estimate of direction preference and breaks the orthogonality between orientation and direction. To resolve this problem, (Kisvarday et al., 2001) proposed to use the “vector maximum method” to evaluate direction selectivity. Yet, this alternative approach suffers from a low angular resolution and remains sensitive to noise (Swindale et al., 2003). A second alternative using the fit of the direction tuning by two von Mises functions, was proposed (Swindale, 1998; Swindale et al., 2003). While this method answers the above concerns, it is however based on the analysis of data recorded in episodic paradigms (i.e. block design). The signal is therefore combined with physiological noise and long recording sessions are needed to increase the signal to noise ratio (by averaging the signal over multiple acquisitions). In some situations, averaging is nevertheless insufficient and additional processing, such as 2D-filtering (Fukuda et al., 2006; Ribot et al., 2006), PCA decomposition (Everson et al., 1997; Gabbay et al., 2000; Stetter et al., 2000; Yokoo et al., 2001), estimation of noise contributions by polynomial subtraction (Ribot et al., 2006) or local similarity minimization (Fekete et al., 2009), must be applied.

Separately, time-locked or periodic techniques have been proposed (Kalatsky and Stryker, 2003; Sornborger et al., 2003; Sornborger et al., 2005). In contrast to episodic paradigms, the periodic approach (i.e. continuous stimulation) combines different conditions by periodically changing the orientation of a stimulus (e.g. grating) and recovers the response by using amplitude and phase information at the stimulation frequency. Experiment duration is thus considerably reduced while more angular conditions are explored since an “infinite” number of orientations can theoretically be presented.

While the periodic method proved to be successful in measuring orientation selectivity in cats (Jha et al., 2005; Kalatsky and Stryker, 2003) and tree shrews (Zepeda et al., 2004), it has never been used to quantify direction selectivity, a fundamental property of visual neurons. In this work, a model-based periodic paradigm is studied for the first time to evaluate direction selectivity from multiple harmonics. A direction index, based on the first and second harmonic of the Fourier decomposition is proposed and tested with different visual stimuli in areas 17,

18 and 21a of the cat, and compared with episodic paradigms. As a demonstration of the exportability, the model is also applied to evaluate the monocular/binocular recipient zones in rodents' primary visual cortex. Part of this work has been previously published in abstract form (Vanni et al., 2007).

METHODS

Model

In this section, notations are introduced for the standard periodic stacking method by including the canonical HRF previously developed (Vanni et al., submitted). The model assumes that measurements are taken with a camera positioned over the cortex to image a zone where activation patterns are expected (Bonhoeffer and Grinvald, 1996). The cortex is illuminated by light at a wavelength for which haemoglobin dominates the absorption (Dunn et al., 2005). The images are recorded continuously to form a dynamical image I(t). Since only one wavelength is used in this work, it is assumed that a combination of deoxyhaemoglobin (HbR) and oxyhaemoglobin (HbO) is measured. For a point in the cortical image, {ij}, the measured attenuation can be modeled as the sum of a physiological signal and the response to the stimuli, i.e.

$$I_{ij}(t)=\alpha_{ij}HRF_{ij}(t) * R_{ij}\{s(t)\}+b_{ij}(t)+e_{ij}(t), \quad (1)$$

where e_{ij} represents the acquisition noise (e.g. generated by the camera), b_{ij}, the physiological signals, namely respiration, cardiac pulsations and vasomotion, and s(t), the stimulation vector defined as s(t)=1 when the stimulation is on, zero otherwise. The specificity of the neuronal response is described by a functional, R_{ij}, describing the normalized response of the neuron to the given stimulus with a response strength α_{ij}, and $HRF_{ij}(t)$ is the haemodynamic response function which convolves the stimuli. It is understood here that the HRF represents the response to a combination of oxy- and deoxy-haemoglobin depending on the illumination wavelength.

In previous work, haemodynamic measurements associated with the above model were used to study the response shape (e.g. the width of the neuronal response in a retinotopic paradigm). This work is extended here by considering a bi-modal stimulation paradigm. Consider the following: a stimulus moving in a direction that continuously rotates at frequency ω_1. If this stimulus is a sinewave grating, with its orientation orthogonal to its direction, the orientation and direction selectivity of neurons can be modeled by a response function taking the form

$$R_{ij}\{s_1(t)+s_2(t)\}=\alpha_{ij}{}^{(1)}R_{ij}{}^{G}\{s_1(t)\}+\alpha_{ij}{}^{(2)}R_{ij}{}^{G}\left\{s_1(t-\frac{\pi}{\omega_1})\right\}. \quad (2)$$

In this formula, the direction selectivity is encoded in the response amplitudes, α_{ij}, which are associated with preferred directions. If both $\alpha_{ij}^{(1)}$ and $\alpha_{ij}^{(2)}$ are equal, neither direction can be distinguished from the other and only the orientation response will be measured. If only one $\alpha_{ij}^{(a)}$ is non- zero, then the direction component dominates the response. This is apparent when taking the Fourier transform of the above expression,

$$R_{ij}\{s_1+s_2\}(\omega)=R_{ij}{}^{G}\{s_1\}(\omega)(\alpha_{ij}{}^{(1)}+\alpha_{ij}{}^{(2)}e^{-i\frac{\pi}{\omega_1}\omega}) \quad (3)$$

where, for simplicity, the function R_{ij}^{G} assumed to be described by a periodic Gaussian centered on the preferred orientation at that location in the cortex, i.e.

$$R_{ij}^{G}\{s\}(\omega)=e^{-\omega^2\sigma^2/2}S_{ij}\{s\}(\omega) \tag{4}$$

and S_{ij} the periodic Dirac response. These Gaussian functions are introduced to model the tuning widths of the underlying neurons. It can be observed that the Fourier transform of (2) will exhibit two peaks, one at ω_1 and one at $\omega_2=2\omega_1$, each having a distinct interpretation in terms of orientation and direction. Consider two special cases. First, if both $\alpha_{ij}^{(a)}$ are equal, (3) will be zero at $\omega=\omega_1$ while non-zero at the second harmonic, $\omega=2\omega_1$. This is the orientation response where the phase can be associated with the preferred orientation. On the other hand, if one $\alpha_{ij}^{(a)}$ is zero, then the first harmonic will have a non-zero response and the phase will correspond to the direction selectivity. Thus, in view of the above model, the amplitude and phase of the responses located at those two peaks can be related to direction selectivity. In fact, it is possible to develop measures that are independent of the contrast or the strength of the response. For example, a quantity of interest, introduced by (Swindale et al., 2003) is the direction index, here referred to as periodic direction index (PDI) because of the nature of the stimulation (i.e in contrast to the episodic direction index (EDI)):

$$PDI_{ij}=\frac{(\alpha_{ij}^{(1)}-\alpha_{ij}^{(2)})}{(\alpha_{ij}^{(1)}+\alpha_{ij}^{(2)})} \tag{5}$$

It measures the direction selectivity of a group of neurons at a given location. Combining (3) and (1), and assuming physiological signal and noise are much lower than the signal at the stimulation frequency, it can be shown that

$$\left|\frac{I_{ij}(\omega_1)}{I_{ij}(2\omega_1)}\right|=\left|\frac{(\alpha_{ij}^{(1)}-\alpha_{ij}^{(2)})}{(\alpha_{ij}^{(1)}+\alpha_{ij}^{(2)})}\right|\left|\frac{HRF(\omega_1)}{HRF(2\omega_1)}\right|e^{\frac{3}{2}\omega_1^2\sigma_{ij}^2}=PDI_{ij}K_{ij}(\omega_1)=PDI' \tag{6}$$

where σ_{ij} describes the temporal width at that stimulation frequency of the modeled Gaussian response of the neurons to orientation and HRF(ω) is the Fourier transform of the HRF. Thus, the remaining factor $K_{ij}(\omega_1)$ depends on both the HRF and σ_{ij} and may vary spatially. However, the experimental observations below indicate that this variation is small when compared to the changes of PDI_{ij} and the scaled index PDI′ defined above will be used in the comparisons below. In theory, the dependence on the tuning width can be removed by using higher harmonics and more complex expressions, an example is:

$$\left|\frac{I_{ij}(\omega_1)}{I_{ij}(2\omega_1)}\left(\frac{I_{ij}(3\omega_1)}{I_{ij}(4\omega_1)}\right)^{-3/7}\right|=\left|\frac{(\alpha_{ij}^{(1)}-\alpha_{ij}^{(2)})}{(\alpha_{ij}^{(1)}+\alpha_{ij}^{(2)})}\right|^{4/7}\left|\frac{HRF(\omega_1)}{HRF(2\omega_1)}\left(\frac{HRF(3\omega_1)}{HRF(4\omega_1)}\right)^{-3/7}\right| \tag{7}$$

but high accuracy up to four harmonics is necessary.

Figure 1 summarizes the previous description. Panel A shows schematic responses associated with three different degrees of direction selectivity when a stimulus of continuously and periodically changing direction is used. When the direction selectivity is high, a response is observed only for a preferred direction, resulting in a unique harmonic at the frequency of the

stimulus. In contrast, when the direction selectivity is absent, the preferred and anti-preferred directions trigger responses of equal amplitudes, resulting in a unique harmonic at twice the frequency of the stimulus (i.e. two responses per rotation). In a general setting, the ratio of the first to the second harmonic (PDI′) provides a measure of the selectivity for direction. Panel B shows a schematic representation of the temporal (B1) and frequency (B2) profiles of neuronal and optical responses. It shows that optical signals result from neuronal responses weighted by the HRF which acts as a low pass filter. As described in the model above (see Eq. 6) and illustrated in panel B, the ratio of the first to second harmonic (PDI) is related to the direction index (PDI) of neurons within the pixel.

Animal preparation

Seven adult cats (2.5 – 3.5 kg), two mice and one rat were used in this study. All procedures were made in accordance with the guidelines of the Canadian Council for the Protection of Animals, and the experimental protocol was accepted by the Ethics Committee of the Université de Montréal. Throughout the experiment, the cats were placed in a stereotaxic frame and artificially ventilated with a mixture of halothane (Fluothane®, 0.6 – 0.8 %) in O_2/N_2O (30%/70%). Muscular relaxation was obtained by the continuous injection of gallamine triethiodide (2%) infused with 5% dextrose in a lactated Ringer's injection solution. End-tidal CO_2, blood pressure, blood oxygen saturation, core temperature, electroencephalogram and electrocardiogram were continuously monitored to evaluate the depth of anaesthesia and the animal welfare. An antibiotic (Tribissen 24%, 0.125 mL/kg/day) was injected s.c. to prevent infections. Pupils were dilated with atropine sulfate 1% (Isopto®) and the eyes were protected using contact lenses of appropriate refractive power (+2). The rat was artificially ventilated with a mixture of isoflurane (Forane®, 1.0 – 1.5 %) in O_2 (100%). Mice were breathing spontaneously in pure O_2 and were anesthetised with urethane (1.25 g/kg, ip).

In cats, a 27 × 20 mm craniotomy was performed over the primary visual cortex at Horsley Clarke coordinates AP −10 to +17 and ML −10 to +10, and the dura was incised to access the cortex. In one case, optical signals were recorded in the neighbouring area 21a. The cat used for this recording was part of another study (Villeneuve et al., submitted). To demonstrate the versatility of the method, the rodent visual cortex was also imaged. In rats, bilateral craniotomies were performed over the primary visual cortex and the dura was left intact. The mouse cortex was imaged through the skull, i.e. without any craniotomy. Imaging chambers were filled with silicone oil (cats) or Agarose in saline (rat and mice) and sealed with a glass plate. At the end of each experiment, the animals were killed by an injection of sodium pentobarbital (cats and rats; Euthanyl, 100mg/kg) or by over inhalation of Isoflurane (mice).

Acquisition and stimulation

The cortex was illuminated at 545 nm to reveal the vascular pattern of the cortical surface and at 630 nm to record the intrinsic signals. Images were recorded with a 12 bits CCD camera (1M60, Dalsa, Colorado Springs, USA) fitted with a macroscopic lens (Nikon, AF Micro Nikkor, 60mm, 1:2.8D).

For direction selectivity measurements, full-screen visual stimuli were generated using a custom made software (STIMPlus) and presented on a 21-in computer screen placed 19 cm in front of the cat eyes. Stimuli were stationary (i.e. static) or drifting (i.e. dynamic) sine-wave gratings (0.15 to 0.5 c/deg) and random-dot kinematograms (RDKs, 0.1 dot per square degree) displayed binocularly and moving at definite velocities (15 or 40 deg/s). For episodic stimulation, the direction of motion was changed pseudo-randomly (16 different values) while for periodic stimulation, it was changed continuously in a counter-clockwise manner at a fixed frequency varying across experiments between 0.006 Hz and 0.167 Hz (see Figure 2B in Kalatsky and Stryker 2003). Continuous acquisition lasted 10 to 30min with a 2–8 Hz sampling

frequency. For episodic stimulation, stimuli were presented during 8s and spaced by 10s intervals after which the next stationary stimulus was presented: the total acquisition time lasted 3 hours with a sampling frequency of 0.6 Hz.

To determine binocular and monocular responses in rodents, full-screen visual stimuli were presented independently to each eye and consisted on a white light emitting diode in direct contact with the eyes (Figure 10, panel A). The surfaces of the LED were drilled to fit the convex curvature of cornea and to stimulate the retina uniformly. Flashes were presented at a frequency of 5Hz during 3s, alternating to the right and left eyes with a period of 12s. Acquisition lasted 10min with a sampling frequency of 8 Hz.

Offline pre-processing and episodic analysis

The data were imported into Matlab (The Mathworks, Nattick, MA) for further analysis. Continuous stimulation signals were subtracted by a normalized temporal pattern of lighting instability (Nassim et al., submitted). For measurements of direction selectivity, frames were band-pass filtered (0.001 – 0.01 μm^{-1}) to remove low and high frequency noise which affects the modular organisation (Fukuda et al., 2006; Jha et al., 2005; Ribot et al., 2006). A Fourier transform was performed on the temporal signal of each pixel to obtain phase and magnitude spectra. To reduce the contribution of the physiological components in our quantitative measurements, baselines (corresponding to the noise floor and obtained by smoothing the spectra with a cut-off of 0.05 Hz) were subtracted from magnitude spectra. The PDI′ was estimated by taking the ratio between the average values of the first and second harmonics in a delimited region of interest. This ratio is related to the periodic direction index (PDI, see eq. 6 of the model) and was compared to the episodic direction index (EDI). Because we did not correct the ratio by the factor $K_{ij}(\omega_1)$, we decided to call the present ratio: PDI′ to avoid any confusion. A local 2D-circular-gradient $\nabla \varphi$ was used to localize fractures in preferred orientation and direction maps (rate of change; (Kim et al., 1999; Kisvarday et al., 2001; Shmuel and Grinvald, 1996; Swindale et al., 2003)), defined by:

$$\nabla\phi = \sqrt{\nabla\cos(\phi)^2 + \nabla\sin(\phi)^2} \tag{8}$$

where

$$\nabla\cos(\phi) = \frac{\partial\cos\phi}{\partial x}\hat{i} + \frac{\partial\cos\phi}{\partial y}\hat{j} \text{ and } \nabla\sin(\phi) = \frac{\partial\sin\phi}{\partial x}\hat{i} + \frac{\partial\sin\phi}{\partial y}\hat{j} \tag{9}$$

with φ, the phase at the first or second harmonic, x and y the vertical and horizontal dimensions (in mm). The decomposition of vertical and horizontal components was used to prevent “circular logic”.

Episodic analysis is based on the vector averaging of responses (Bonhoeffer and Grinvald, 1996; Shmuel and Grinvald, 1996) or Von Mises fitting method (Swindale, 1998; Swindale et al., 2003). For orientation, trials were summed for the same-orientation-opposite-direction. Orientation and direction single condition maps (averages of 30–40 trials) were then band-pass filtered. The general framework of the Von Mises fitting method described in (Swindale et al., 2003) was used to recover preferred orientation, preferred direction, magnitude of orientation selectivity and episodic direction index (EDI) defined as:

$$EDI = \frac{|A_1 - A_2|}{A_1 + A_2} \tag{10}$$

where A_1 is the magnitude for preferred and A_2 for anti-preferred directions (Swindale et al., 2003).

The degree of similarity between maps was measured by computing correlation coefficients. In the case of polar maps (e.g. direction and orientation maps), a transformation in polar coordinates was done prior to the calculation, and the r-values corresponded to the summation of the r-values of sine and cosine components of the maps. Given the large number of pixels, the statistical inference (p) could not be considered as valid and consequently will not be shown.

Based on the linearity of the response, it is possible to estimate the HRF profile in the frequency domain by the assumption:

$$|HRF(\omega)| \approx k \frac{|I_{ij}(\omega)|}{(N+1)} \tag{11}$$

with N, the number of presentation of the stimulus and k, a factor described in (Vanni et al., submitted).

RESULTS

First and second harmonics to evaluate direction and orientation selectivity

The first series of experiments confirmed that the Fourier transform can be used to reveal direction selectivity from the profile of the neuronal response. Figure 2 shows typical recordings in one location in area 18 of the cat for three stimuli evoking different degrees of direction selectivity. Panel A shows the profile of the response with periodic and episodic paradigms for three distinct stimuli: RDK (15 deg/s), static and dynamic gratings. For each stimulus, periodic and episodic paradigms provided comparable response profiles with the exception of a slight delay between the periodic and the episodic paradigms. This delay is presumed to originate from the hemodynamic response. Panel B provides the Fourier transform of the profiles obtained with the periodic paradigm. In B_1, stimulation with a static grating does not evoke any direction components. This results in two equal responses per rotation at the preferred orientation leading to a lack of response at the first harmonic and a strong response at the second (PDI′ = 0). A small peak at the fourth harmonic was also observed. As described in (Vanni et al., submitted), this component is attributable to the profile of the neuronal response (i.e. tuning bandwidth). In B_2, RDK, which are known to yield robust direction components, evoked a strong response at the first harmonic. A small peak at the second harmonic was also observed (PDI′ = 3.6). It is noticeable that this second harmonic derives from direction selectivity (i.e. in reference to the response at the anti-preferred direction) but can also originate, in part, from the direction tuning bandwidth as previously mentioned for orientation. Increasing the velocity of the RDK did not provide a significantly different profile (40deg/s, data not shown). Finally, in B_3, stimulation with a dynamic grating evokes both direction and orientation components causing a response for the preferred but also for the anti-preferred direction with weaker amplitude. The result was the presence of components both at the first and second harmonics (PDI′ = 0.5 and 0.7 in two separate measures).

Spatial maps of first and second harmonics for these three stimuli are shown in Figure 3. Panel 1 shows the response for a static grating. In agreement with the spectra presented above, there

was no response at the first harmonic (panel B1) whereas a clear orientation selectivity map was imaged at the second harmonic (i.e. presence of domains and pinwheels, panel C1). This led to an absence of direction selectivity and a PDI′ close to zero (panel D). At the location of pinwheels, the magnitude of the second harmonic was always smaller than that observed in the domains. Panel 2 shows the response for RDK. A clear modular organisation was observed at the first harmonic which is likely to correspond to the direction selectivity map (panel B2 and C2). The corresponding PDI′ map has high values associated with high direction selectivity (panel D2). Panel 3 shows the response to a dynamic grating. A clear modular organisation was observed at the first harmonic, similar to that obtained with RDK in panel B2 (panel B3). A clear modular organisation was also observed at the second harmonic (panel C3) and was comparable to the one found with the static grating in panel C1. These observations support the idea that the first harmonic can be considered as carrying direction and the second harmonic, orientation. Finally, due to the presence of orientation components, the values of the PDI′ map were weaker than those with a RDK stimulus (panel D3).

Table 1 reports the similarity of phase maps as a function of the recording time. When the recording was split into two equal sub-recordings, the resulting maps were comparable (shaded row). These results confirmed that those maps cannot be ascribed to background noise. The maps obtained during a 30min recording period were compared with those acquired with periods inferior to 30min in duration. The goal was to evaluate the minimum amount of time necessary to obtain a map similar to the reference map (i.e., that acquired in 30min). The signal to noise ratio (SNR) of each recording session was also evaluated. It was defined as the peak of the signal at the first or second harmonic divided by the noise floor. The threshold value was defined by having a SNR greater than two. Results revealed that reliable second harmonic maps (orientation) can be imaged in only 1–2min while first harmonic maps (direction) can be obtained around 10–15min, a value acceptable when short-recording sessions are mandatory. The same quality of images was indeed reached 5–10 times faster than with the episodic paradigm (data not shown).

The maps obtained above (periodic paradigm) were compared to those acquired with an episodic paradigm (Figure 4). Panels A and B show orientation selectivity maps for dynamic and static gratings. These maps were similar to each other and to that of the second harmonic shown in Figure 3 (panels C1, C3). Panels C and D display direction selectivity maps for both dynamic gratings and RDK. These maps were also similar to each other and to that of the first harmonic shown in Figure 3 (B2 and B3). As expected, a clear relationship was observed between the phase of the second harmonic and the preferred orientation (r=0.87 for dynamic and r=0.82 for static grating, panel E), and between the phase of the first harmonic and the preferred direction (r=0.58 for dynamic grating and r=0.59 for RDK, panel F). Panel G shows a linear relationship between the magnitude at the second harmonic and the orientation magnitude (r = 0.85 and r = 0.72 for dynamic and static gratings). Finally, panel H shows the relationship between the PDI′ and the EDI. When RDK and dynamic gratings indexes are pooled together, a clear relation is observable: pixels from RDK had higher values while those from dynamic grating had lower values (r = 0.42). The PDI′ was higher than the EDI (by one order of magnitude). This is explained by the weighting of the PDI and a factor related to HRF and bandwidth (see Eq. 6 of the model) which act as a low-pass filter, promoting the first harmonic more than the second and thus, increasing PDI′ (see Figure 1, Figure 8, panel C and (Vanni et al., submitted)). Similar results were observed when the periodic paradigm was compared to the vector sum measurements (for orientation; r = 0.82 and r = 0.87 for static and dynamic gratings respectively, for direction; r=0.73 and r = 0.69 for dynamic grating and RDK, respectively) or vector max computation (for orientation; r = 0.64 and r = 0.72 for static and dynamic gratings; and for direction; r = 0.51 and r = 0.55 for dynamic grating and RDK).

To further confirm that first and second harmonics can provide information on direction and orientation, cross validation between these components was evaluated as an internal validation shown in Figure 5. A good correlation was observed for the phase (r=0.95, panel C) and magnitude (r=0.98, panel A) of the second harmonic between static and dynamic gratings even though direction components were present in the second stimulus. Similarly, there was a good correspondence between the phase of the first harmonic for RDK and that for dynamic gratings despite the existence of orientation components in the latter (r = 0.85, panel B). The relationship between PDI′ for RDK and dynamic gratings is presented in panel D (r = 0.47). Because of the presence of orientation components contributing to the second harmonic, the PDI′ was one order of magnitude lower for dynamic gratings than for RDK.

Correlation between the phase of the first and the second harmonics was also evaluated to determine the angular relationship between orientation and direction (panel E). When tested with a dynamic grating, a correlation was observed between the phase of the first and the second harmonic. As shown by (Swindale et al., 2003) the relationship revealed an orthogonality: each second harmonic phase (orientation) was associated with a first harmonic phase (direction) shifted by $\pi/2$ or $3\pi/2$ in reference to the former. However, compared to (Swindale et al., 2003) the relationship was noisy (points in Figure E, r = 0.25). The exclusion of pixels of fracture and low direction selectivity considerably increased the correlation (circles in Figure E, r = 0.66).

Fractures in direction map

Considering the phase of the first harmonic as an evaluation of the preferred direction map, we examined its relationship with the direction selectivity map PDI′ (Figure 6). As explained in panel A, the hypothesis was that, in fractures revealed by a 2D-gradient; (rate of change (Kim et al., 1999;Kisvarday et al., 2001;Shmuel and Grinvald, 1996;Swindale et al., 2003)) direction selectivity is expected to be low. This should provoke a decrease of the first harmonic associated with direction without affecting the second, which is associated with orientation. The phase of the first harmonic (panel B) was used to calculate the 2D-gradient (panel C) as previously computed in previous studies (Kim et al., 1999;Kisvarday et al., 2001;Shmuel and Grinvald, 1996;Swindale et al., 2003). A high gradient was associated with high variations of the direction preference. The relationship between gradient and PDI′ (panel D) in regions of interest indicated by white boxes (and their magnification) is presented in panel E. An inverse relationship is observed, meaning that high gradients (i.e. fractures) are associated with low direction selectivity, as previously stated. The decrease of the PDI′ was caused by a reduction of first harmonic, while the second remained constant, i.e. without an effect on orientation response, as shown in panel F (PDI′ = 0.6 in domains and 0.2 in fracture locations). These results were obtained with a dynamic grating but the same observation was made with RDK (data not shown).

Measures of direction selectivity

To further demonstrate that PDI′ can be used to evaluate direction selectivity, the temporal frequency of the grating direction was modified (Figure 7). Neurons in area 18 exhibit temporal frequency tuning that should be detectable with optical imaging. Panel A presents the spectra obtained for different temporal frequencies. No peak at the first harmonic was observed at 0 Hz because no direction component was present (static grating). At 2, 4 and 6 Hz, the first harmonic can be used to calculate the PDI′ shown in panel B. Despite the limited number of temporal frequencies tested, a temporal frequency tuning curve can be distinguished with a maximum PDI′ between 2 and 4 Hz. Table 2 shows that there was no differences in the pattern of the maps across temporal frequencies (maps not shown).

The range of stimulus frequencies to assess the PDI′ was evaluated with a dynamic grating (Figure 8). Since the signal in optical imaging is a weighting of the neuronal response and HRF (see Figure 1), and that the HRF is delimited in the frequency space (i.e. low frequency band), the magnitude of the harmonics should be influenced by the stimulus frequency. The responses for different stimulus frequencies, ranging from 0.006 Hz to 0.167 Hz, were evaluated (panel A). In every case, the first and the second harmonics could be discriminated and it was possible to calculate the PDI′ (panel B). The optimal range of stimulus frequencies, defined by having a signal to noise ratio greater than two, was located between ~0.01 Hz and ~0.05 Hz. At higher frequencies, the second harmonic is filtered by the HRF and/or can be influenced by vasomotor waves (present at 0.1 Hz). At lower frequencies, the first harmonic can be affected by slow fluctuations (i.e. DC components clearly visible under 0.02 Hz) and noise due to the poor number of repetitions in a delimited recording time. Panel C shows an example of the HRF profile obtained from the data presented in panels A. The domain of frequency associated with the orientation mapping signal was localized in the lower range of frequencies (less than 0.04 Hz; low-pass profile). In contrast, we previously showed that the HRF for global activation had a band-pass profile, localized around 0.1–0.15 Hz (Vanni et al., submitted). The homogeneity of the HRF profile was compared for every pixel (panel D) and exhibited uniformity throughout the cortex, in accordance with our previous findings. Consequently, according to Eq. 6, the variations of PDI′ do not come from a change in the HRF, but rather from neuronal properties (i.e. direction selectivity).

Despite some variability in the measures, the PDI′ can be a reliable measure of the differences in direction selectivity across cortical areas or after experimental manipulations (e.g., pharmacological modulation). This is demonstrated in Figure 9 where the PDI′ was used to evaluate and compare direction selectivity in brain areas along the dorsal and ventral pathways (Figure 9, panel A). In comparison to area 18, areas 17 and 21a are considered to be involved in form (i.e. orientation) rather than motion analysis (direction). Panel B shows the spectrum of the response recorded in area 21a, a high-order area of the ventral stream where orientation domains are present with low direction selectivity (Huang et al., 2006;Villeneuve et al., submitted). Panel C displays the first and the second harmonic maps and no evidence of activation at the first harmonic could be observed. However, orientation domains were present at the second harmonic. This orientation map was validated by recordings with episodic paradigm (data not shown). PDI′ of the experiment reported here was 0.1 (stimulus frequency = 0.008Hz, spatial frequency of the grating: 0.2c/deg, temporal frequency: 3Hz). Similar low values were reported in other stimulus condition (PDI′ = 0.2 and 0.3 for a stimulus frequency of 0.017Hz, spatial frequency of the grating: 0.1c/deg, temporal frequency: 4Hz, maps and spectra not shown). Values of PDI′ were always lower than those in area 18 (see grey points in Figure 8, panel B).

Panel D shows the spectra of the response recorded in area 17 and 18 for dynamic gratings with parameters set to optimally activate area 17 neurons (stimulus frequency = 0.025Hz, spatial frequency of the grating: 0.5c/deg, temporal frequency: 3Hz). Despite the fact that the spatial frequency used was not optimal for neurons in area 18, a strong response at the first harmonic relative to the second was observed (PDI′ 1) in comparison to that found in area 17 (PDI′ = 0.4 and see white points in Figure 8, panel B). Similar results were observed in other experiments but in some cases, differences of PDI′ between areas 17 and 18 were smaller (data not shown). Panels E1 and E2 show the response at the first and the second harmonics and reveal the reduced response at the first harmonic in area 17 (e.g., when compared to area 18 in panels B3 and C3 of Figure 3). Note that the scale of magnitude displayed was optimized to appreciate the whole range of signal amplitude in area 17 preventing then a clear observation of the low signals present in area 18 in this condition of stimulation.

Demonstration of versatility of the bimodal modulation: measures of monocular and binocular responses

The principle of bimodal modulation for direction selectivity in cats was exploited to map other parameters such as the "binocular selectivity" of the visual cortex in rodents (Figure 10). In this animal order, each eye is indirectly connected to the contralateral monocular cortex (Adams and Forrester, 1968; Cang et al., 2005; Drager, 1975; Gias et al., 2005; Kalatsky and Stryker, 2003; Mangini and Pearlman, 1980; Schuett et al., 2002; Wagor et al., 1980). However, parts of the retinopetal projections, associated with the frontal visual field, are ipsilateral and project to the binocular region of the cortex (panel A). In this experiment, LEDs were used to stimulate each eye in an alternate fashion. Responses were expected to be unimodal in the monocular part of the cortex and bimodal in the binocular area (i.e. patterns similar to "high" and "low direction selectivity" in Figure 1, respectively). This was tested on mice (panels 1) and rats (panels 2). Panels C display the responses at the first harmonic. Activations of the visual cortex were clearly visible in both animals with two distinct phases corresponding to the activation of each eye (i.e. green and magenta colors). Panels D display the responses at the second harmonic. Activations were also clearly visible and slightly lateral. The phase was homogeneous throughout both hemispheres because the LED stimulus equally activates each binocular cortex. These results provide evidence that the second harmonic is linked to binocular information whereas the first harmonic carries monocular information. The ratio of the second to first harmonics was used to reveal the degree of "binocularity". This ratio was computed in regions where activation was visible (ROI highlighted in panels E). As previously assumed, a high ratio (i.e. high "binocularity") was present in the lateral part of the visual cortex in both species. The spectra presented in panels F show the ratio in both species (1.2 (mouse) and 0.7 (rat) in the binocular zones and 0.1 (mouse) and 0.3 (rat) in monocular zones).

DISCUSSION

This study indicated that, in combination with continuous stimulation, first and second harmonics of the Fourier decomposition of optical signals can be successfully used to reveal direction selectivity. While the phase and magnitude of the second harmonic were associated with orientation components (i.e. preferred orientation and strength), the phase of the first harmonic was driven by the preferred direction. The observations reported in this paper confirm that under appropriate conditions, the ratio of the first/the second harmonics can be used as an evaluation of the direction selectivity similar to a "direction index" in an episodic paradigm. These results are thus in accord with those obtained from episodic paradigms but can be obtained in shorter recording sessions.

The ratio of the first/the second harmonic, named uncorrected periodic direction index (PDI′) in the present study, was measured in area 18 using both gratings and RDK. The quantification of PDI′ was observed to vary with the grating's temporal frequency and was greater with RDK. The PDI′ was small in fractures of preferred direction maps corresponding to low direction selectivity loci. The PDI′ was also smaller in areas of the ventral pathway that are less implicated in direction selectivity, such as areas 17 and 21a. Finally, bimodal modulation was used to reveal the binocular selectivity of the visual cortex of rats and mice. Unimodal and bimodal responses were associated with first and second harmonics respectively and the ratio of the second/first harmonic could be used as a measure of "binocularity".

Periodic stimulation

Combining continuous recording and spectral decomposition represents a powerful method given that the optical signal can be easily discriminated from periodic physiological noise: heartbeat (~3 Hz), respiration (~0.5 Hz) and vasomotion (~0.1 Hz in (Mayhew et al., 1996), ~0.14 Hz in the present study). The recording time is thus considerably reduced. This approach

has proved to be successful for acquiring clear orientation maps in very short sessions either by optical imaging (in the order of minutes; present study, (Jha et al., 2005; Kalatsky and Stryker, 2003; Zepeda et al., 2004)) or other modalities such as fMRI (Fukuda et al., 2006; Moon et al., 2007). Nevertheless, the low-frequency domain of the HRF requires stimulating at slow frequencies (between 0.01 Hz and 0.05 Hz) and it is preferable to use a recording time longer enough to have a sufficient number of repetitions to discriminate the first harmonic. To estimate direction, associated with the first harmonic, 10 to 30min of recording was found to be appropriate (this is 6 to 20 times shorter than with episodic paradigms). Thus the continuous paradigm represents a powerful method for studying the impact of experimental manipulations on cortical functioning. For example, it could be used to investigate the feedback influences of high-level areas on orientation and direction selectivity in primary areas by rapid and reversible pharmacological deactivation of the projecting area (Galuske et al., 2002; Huang et al., 2004; Liang et al., 2007; Shen et al., 2008). It could also be a powerful tool to measure neurons' visual functions which necessitates a large number of conditions such as contrast sensitivity functions.

Despite the spectral decomposition, 2D-noise contributions are present in harmonics related to the stimulus. Here, a spatial band-pass filtering has been applied to each frame of the recording prior to the Fourier transform (Fukuda et al., 2006; Jha et al., 2005). This method of noise reduction presumes an "a priori" knowledge of the spatial pattern of domains and can modify quantifications (Ribot et al., 2006; Villeneuve et al., submitted). This is not likely the case as (Swindale et al., 2003) demonstrated that smoothing (i.e. low-pass filtering) does not significantly affect the pattern of orientation maps.

Information carried by harmonics

As in previous studies (Jha et al., 2005; Kalatsky and Stryker, 2003; Zepeda et al., 2004), second harmonic information was exploited to reveal orientation components with both static and dynamic gratings. The innovative aspects of the present study are the demonstration that the first harmonic can be used to reveal direction and that the ratio of the magnitude of the first to the second harmonic (PDI′) represents a powerful measure of direction selectivity. Indeed, this ratio informs about the selectivity of the response to one direction in comparison with the opposite. Nonetheless, as shown in Eq. (6), this ratio (PDI′) is not a direct measure of the direction selectivity (PDI) as used in (Swindale et al., 2003). To have the exact value, HRF factors must be introduced by canonical estimation or physiological evaluation (Vanni et al., submitted). Despite this issue, the PDI′ is appropriate in studies where hemodynamic components are not expected to change (e.g. pharmacological and cooling inactivation).

As previously described, the phase of the first and second harmonics can also be used to reveal direction and orientation preferences. As expected, an orthogonal relationship between orientation and direction was observed (Henry et al., 1974; Kim et al., 1999; Kisvarday et al., 2001; Ribot et al., 2008; Shmuel and Grinvald, 1996; Swindale et al., 2003). While periodic stimulation is known to have a better SNR (Kalatsky and Stryker, 2003), the orthogonal relationship was considerably noisier than that found with Von Mises fitting. A possible explanation is that the first and second harmonics alone do not provide an exact evaluation of the preferred direction and orientation. More precisely, a first possibility is that higher harmonics, related to the shape of the response, should be considered (see third and fourth harmonics in Figure 2, panel B3). This is also in accordance with (Swindale, 1998) who concluded that the cosine function does not fit very well to the orientation tuning function. The cosine function is indeed the function used in "vector sums" as well as Fourier decomposition when restricted to the first harmonic. Regardless, (Worgotter and Eysel, 1987) reported that higher harmonics contribute only remotely to the shape of the polar plot. A second possibility is that the signal at the first harmonic with a dynamic grating is the consequence of both

preferred and anti-preferred responses (See Eq. 6 of the model). Indeed, while the response in the preferred direction dominates the phase at the first harmonic it could be contaminated by the anti-preferred direction response. However, the relationship remained noisy when the phase of the first harmonic of a RDK (i.e. to minimize the anti-preferred response) was compared to the phase of the second harmonic of a static grating (i.e. to eliminate the direction response). A third possibility is that the model assumes orientation to be truly orthogonal to direction but this relationship may not be as rigid. In the future, bimodal modulation would benefit from implementing and validating a model exploiting higher harmonics.

Despite the above statements, a good correspondence was observed between the present periodic paradigm and previous episodic ones, regardless of the controversies about direction estimation (Kim et al., 1999; Kisvarday et al., 2001; Ribot et al., 2008; Shmuel and Grinvald, 1996; Swindale et al., 2003). The Fourier transform on episodic electrophysiological data described in (Worgotter and Eysel, 1987) does not exploit the main advantage of the periodic paradigm: i.e. the discrimination of periodic responses from noise. Moreover, the long recording session in episodic paradigms requires minimizing the number of conditions. For example, orientation maps were often constructed from only four orientations whereas more than eight would be needed to obtain a reliable assessment of orientation selectivity (Womelsdorf et al., 2001). Such requirement would be met in a periodic paradigm where an infinite number of stimuli are presented (Kalatsky and Stryker, 2003).

Direction selectivity

Area 18 is located along the dorsal stream and is implicated in motion and depth perception (Lomber, 2001; Shmuel and Grinvald, 1996; Swindale et al., 2003). In this study, we have compared direction selectivity measures in area 18 with those obtained in areas of the ventral stream (area 17 and 21a) which are known to be preferentially involved in form rather than motion perception (Lomber, 2001; Villeneuve et al., submitted). Such comparison was never based on optical imaging data and it offered us the opportunity to evaluate the sensitivity of our paradigm in assessing direction in areas with low directional preferences. The PDI's measured in area 21a were always weaker than those in area 18. This is in accordance with previous optical imaging studies which showed that only orientation maps are present in area 21a (Huang et al., 2006; Villeneuve et al., submitted), and with electrophysiological findings which indicate a low direction selectivity of area 21a neurons (Dreher et al., 1993). A smaller PDI′ was also reported in area 17 in comparison to area 18 but the difference was less than that observed between areas 21a and 18. This may be due to the fact that, at the level of area centralis representation, the number of direction selective cells and their direction selectivity is greater in area 18 than in 17 (Orban et al., 1981). However, the differences between the two areas is not considerable and may stem from the fact that the portion of area 17 accessible through the craniotomy was very small and could correspond to areas 17–18 transition zone where optical direction properties can be "hybrid" (Ohki et al., 2000; Rochefort et al., 2007). One may also suggest that the HRF may be different in area 17 and 18, affecting the harmonic distribution and thus the PDI′. However, as shown here and in (Vanni et al., submitted), the HRF is uniform throughout the primary visual cortex.

The pattern of direction selectivity was also evaluated across area 18 and compared between domains and singularities. The amplitude of the second harmonic was low near orientation singularities (pinwheels), revealing a weaker orientation response as previously described (Swindale et al., 2003). Furthermore, the PDI′ was found to be lower in direction singularities (fractures). This is in agreement with previous reports in optical imaging showing low direction selectivity in fracture locations in optical imaging (Shmuel and Grinvald, 1996; Swindale et al., 2003) and at cellular levels (Ohki et al., 2005).

Special attention is needed with respect to the rotational nature of the paradigm. An additional and artifactual velocity is present which varies as a function of the eccentricity of the rotation. This artifactual velocity is defined as $Va = 2\pi EF$ where E is the eccentricity in degrees and F is the frequency of rotation in Hz. For example, Va was 1.6 deg/s at 10 deg of eccentricity for a frequency of 0.025 Hz (1/40s). When the spatiotemporal parameters of the grating presented was optimal for area 18 (0.15 c/deg, 4Hz) the velocity of the stimulus was 26.6 deg/s and the artifactual velocity was negligible (6% of variation at 10 deg of eccentricity). In contrast, when parameters were optimal for area 17 (0.5 c/deg, 2Hz) the velocity of the stimulus was 4 deg/s and the artifactual velocity affected the homogeneity of the stimulus speed (40% of variation). This means that, at 10 deg of eccentricity, the apparent velocity was 2.4 deg/s and was, in the opposite position, 5.6 deg/s. Thus one should reduce the frequency of rotation to minimize this effect. We showed that excellent direction quantification can be obtained down to 0.01 Hz (1/100s).

Binocularity

Given the success of the bimodal modulation in evaluating direction selectivity, the technique was adapted for the assessment of the binocular/monocular areas of the primary visual cortex in rodents. Clearly, the first harmonic of the signal was related to the monocular response, and the second to the binocular response. Here again, the ratio of the second to first harmonics can be used as a measure of “binocularity” (i.e. tendency to respond equally to both eyes). This measure is similar to the ratio (C−I)/(C+I) described in (Cang et al., 2005) but the present method has the advantage of stimulating the whole retina of both eyes during the same recording session, reducing the contribution of physiological variations between two recording sessions. However, as stated in the model, our ratio is not a direct evaluation of (C−I)/(C+I) because of the weighting by the HRF. Nevertheless, the second to first harmonic ratios can be used to delineate binocular and monocular zones and study their relative sized after experimental manipulations such as monocular light deprivation. Our results are in agreement with the binocular/monocular mappings in the visual cortex of mice (Cang et al., 2005; Drager, 1975; Kalatsky and Stryker, 2003; Mangini and Pearlman, 1980; Schuett et al., 2002; Wagor et al., 1980) and rats (Adams and Forrester, 1968; Gias et al., 2005). The visual cortex has a large monocular zone (related to the contralateral eye) surrounded laterally by binocular zones displaying a preference for the contralateral eye. An alternative approach could be the stimulation of both eyes with distinct frequencies, with the assumption of linearity of response of the Fourier transform (Kalatsky et al., 2006; Vanni et al., submitted). In that case, the responses at both frequencies are the combination of the neuronal responses and the HRF, the latter contributing differently at each frequency (see Figure 1). Therefore, the use of this alternative approach necessitates the characterisation of the HRF to normalize the responses.

Conclusions

This work presents evidence that bimodal modulation in periodic stimulation can be used to evaluate direction selectivity and that it can be exported to other properties such as binocularity. This new paradigm could be adapted to other visual modalities such as color coding or retinal disparity and to the investigation of multisensory processing (e.g. visual vs. auditory input). In the future, this paradigm could be translated to other optical imaging modalities aimed at the investigation of the visual cortex organization, such as autofluorescence flavoprotein imaging, voltage sensitive dyes, laminar optical tomography or in vivo two photon microscopy, (Blasdel, 1992; Hillman et al., 2007; Husson et al., 2007; Ohki et al., 2005). Exportation to high resolution fMRI is also easily conceivable (Fukuda et al., 2006; Moon et al., 2007).

Acknowledgments

This work was supported by NSERC, CIHR MOP-14825, and NEI R01EY016155 grants to C.C. and a NSERC grant to F.L. FRSQ provided part of C.C.'s salary (chercheur national program). JP was supported by a NSERC scholarship. M.P.V. was supported in part by "Foreign Affairs and International Trade" and "Faculté des études supérieures" fellowships. We thank Martin Villeneuve, Karine Minville and Marilyse Piché for their helpful assistance during experiments. We thank Jonathan Roy, Bertrand Guay-Paquet, Nicolas Rousseau-Dupuis, Marc Melillo and François Vaillancourt for building the stimulus generator and LED device.

References

Adams AD, Forrester JM. The projection of the rat's visual field on the cerebral cortex. Q J Exp Physiol Cogn Med Sci 1968;53:327–336. [PubMed: 5188317]

Blasdel GG. Differential imaging of ocular dominance and orientation selectivity in monkey striate cortex. J Neurosci 1992;12:3115–3138. [PubMed: 1494950]

Bonhoeffer T, Grinvald A. Iso-orientation domains in cat visual cortex are arranged in pinwheel-like patterns. Nature 1991;353:429–431. [PubMed: 1896085]

Bonhoeffer, T.; Grinvald, A. Optical imaging based on intrinsic signal- the methodology. In: Toga, AW.; Mazziotta, JC., editors. Brain Mapping: The Methods. 1996.

Cang J, Kalatsky VA, Lowel S, Stryker MP. Optical imaging of the intrinsic signal as a measure of cortical plasticity in the mouse. Vis Neurosci 2005;22:685–691. [PubMed: 16332279]

Drager UC. Receptive fields of single cells and topography in mouse visual cortex. J Comp Neurol 1975;160:269–290. [PubMed: 1112925]

Dreher B, Michalski A, Ho RH, Lee CW, Burke W. Processing of form and motion in area 21a of cat visual cortex. Vis Neurosci 1993;10:93–115. [PubMed: 8424929]

Dunn AK, Devor A, Dale AM, Boas DA. Spatial extent of oxygen metabolism and hemodynamic changes during functional activation of the rat somatosensory cortex. Neuroimage 2005;27:279–290. [PubMed: 15925522]

Everson R, Knight BW, Sirovich L. Separating spatially distributed response to stimulation from background. I. Optical imaging. Biol Cybern 1997;77:407–417. [PubMed: 9433755]

Fekete T, Omer DB, Naaman S, Grinvald A. Removal of spatial biological artifacts in functional maps by local similarity minimization. J Neurosci Methods 2009;178:31–39. [PubMed: 19101591]

Frostig RD, Lieke EE, Ts'o DY, Grinvald A. Cortical functional architecture and local coupling between neuronal activity and the microcirculation revealed by in vivo high-resolution optical imaging of intrinsic signals. Proc Natl Acad Sci U S A 1990;87:6082–6086. [PubMed: 2117272]

Fukuda M, Moon CH, Wang P, Kim SG. Mapping iso-orientation columns by contrast agent-enhanced functional magnetic resonance imaging: reproducibility, specificity, and evaluation by optical imaging of intrinsic signal. J Neurosci 2006;26:11821–11832. [PubMed: 17108155]

Gabbay M, Brennan C, Kaplan E, Sirovich L. A principal components-based method for the detection of neuronal activity maps: application to optical imaging. Neuroimage 2000;11:313–325. [PubMed: 10725187]

Galuske RA, Schmidt KE, Goebel R, Lomber SG, Payne BR. The role of feedback in shaping neural representations in cat visual cortex. Proc Natl Acad Sci U S A 2002;99:17083–17088. [PubMed: 12477930]

Gias C, Hewson-Stoate N, Jones M, Johnston D, Mayhew JE, Coffey PJ. Retinotopy within rat primary visual cortex using optical imaging. Neuroimage 2005;24:200–206. [PubMed: 15588611]

Grinvald A, Lieke E, Frostig RD, Gilbert CD, Wiesel TN. Functional architecture of cortex revealed by optical imaging of intrinsic signals. Nature 1986;324:361–364. [PubMed: 3785405]

Henry GH, Bishop PO, Dreher B. Orientation, axis and direction as stimulus parameters for striate cells. Vision Res 1974;14:767–777. [PubMed: 4422599]

Hillman EM, Devor A, Bouchard MB, Dunn AK, Krauss GW, Skoch J, Bacskai BJ, Dale AM, Boas DA. Depth-resolved optical imaging and microscopy of vascular compartment dynamics during somatosensory stimulation. Neuroimage 2007;35:89–104. [PubMed: 17222567]

Huang L, Chen X, Shou T. Spatial frequency-dependent feedback of visual cortical area 21a modulating functional orientation column maps in areas 17 and 18 of the cat. Brain Res 2004;998:194–201. [PubMed: 14751590]

Huang L, Shou T, Chen X, Yu H, Sun C, Liang Z. Slab-like functional architecture of higher order cortical area 21a showing oblique effect of orientation preference in the cat. Neuroimage 2006;32:1365–1374. [PubMed: 16798018]

Husson TR, Mallik AK, Zhang JX, Issa NP. Functional imaging of primary visual cortex using flavoprotein autofluorescence. J Neurosci 2007;27:8665–8675. [PubMed: 17687044]

Jha SK, Jones BE, Coleman T, Steinmetz N, Law CT, Griffin G, Hawk J, Dabbish N, Kalatsky VA, Frank MG. Sleep-dependent plasticity requires cortical activity. J Neurosci 2005;25:9266–9274. [PubMed: 16207886]

Kalatsky VA, O'Connor EM, Tcheslavski GV, Kalatsky V. Concurrent multidimensional imaging of visual space representations in mouse visual cortex by Fourier optical imaging of intrinsic signals. SfN abstract prog 2006:503.9.

Kalatsky VA, Stryker MP. New paradigm for optical imaging: temporally encoded maps of intrinsic signal. Neuron 2003;38:529–545. [PubMed: 12765606]

Kim DS, Matsuda Y, Ohki K, Ajima A, Tanaka S. Geometrical and topological relationships between multiple functional maps in cat primary visual cortex. Neuroreport 1999;10:2515–2522. [PubMed: 10574362]

Kisvarday ZF, Buzas P, Eysel UT. Calculating direction maps from intrinsic signals revealed by optical imaging. Cereb Cortex 2001;11:636–647. [PubMed: 11415966]

Liang Z, Shen W, Shou T. Enhancement of oblique effect in the cat's primary visual cortex via orientation preference shifting induced by excitatory feedback from higher-order cortical area 21a. Neuroscience 2007;145:377–383. [PubMed: 17223276]

Lomber SG. Behavioral cartography of visual functions in cat parietal cortex: areal and laminar dissociations. Prog Brain Res 2001;134:265–284. [PubMed: 11702548]

Mangini NJ, Pearlman AL. Laminar distribution of receptive field properties in the primary visual cortex of the mouse. J Comp Neurol 1980;193:203–222. [PubMed: 6776165]

Mayhew JE, Askew S, Zheng Y, Porrill J, Westby GW, Redgrave P, Rector DM, Harper RM. Cerebral vasomotion: a 0.1-Hz oscillation in reflected light imaging of neural activity. Neuroimage 1996;4:183–193. [PubMed: 9345508]

Moon CH, Fukuda M, Park SH, Kim SG. Neural interpretation of blood oxygenation level-dependent fMRI maps at submillimeter columnar resolution. J Neurosci 2007;27:6892–6902. [PubMed: 17596437]

Nassim MY, Vanni MP, Casanova C. New Tools for Mapping the Rat Visual Cortex and Superior Colliculus by Optical Imaging. Experimental Brain Research. submitted

Ohki K, Chung S, Ch'ng YH, Kara P, Reid RC. Functional imaging with cellular resolution reveals precise micro-architecture in visual cortex. Nature 2005;433:597–603. [PubMed: 15660108]

Ohki K, Matsuda Y, Ajima A, Kim DS, Tanaka S. Arrangement of orientation pinwheel centers around area 17/18 transition zone in cat visual cortex. Cereb Cortex 2000;10:593–601. [PubMed: 10859137]

Orban GA, Kennedy H, Maes H. Response to movement of neurons in areas 17 and 18 of the cat: direction selectivity. J Neurophysiol 1981;45:1059–1073. [PubMed: 7252530]

Ribot J, Tanaka S, O'Hashi K, Ajima A. Anisotropy in the representation of direction preferences in cat area 18. Eur J Neurosci 2008;27:2773–2780. [PubMed: 18489580]

Ribot J, Tanaka S, Tanaka H, Ajima A. Online analysis method for intrinsic signal optical imaging. J Neurosci Methods 2006;153:8–20. [PubMed: 16321445]

Rochefort NL, Buzas P, Kisvarday ZF, Eysel UT, Milleret C. Layout of transcallosal activity in cat visual cortex revealed by optical imaging. Neuroimage 2007;36:804–821. [PubMed: 17475512]

Schuett S, Bonhoeffer T, Hubener M. Mapping retinotopic structure in mouse visual cortex with optical imaging. J Neurosci 2002;22:6549–6559. [PubMed: 12151534]

Shen W, Liang Z, Shou T. Weakened feedback abolishes neural oblique effect evoked by pseudo-natural visual stimuli in area 17 of the cat. Neurosci Lett 2008;437:65–70. [PubMed: 18420348]

Shmuel A, Grinvald A. Functional organization for direction of motion and its relationship to orientation maps in cat area 18. J Neurosci 1996;16:6945–6964. [PubMed: 8824332]

Sornborger A, Sailstad C, Kaplan E, Sirovich L. Spatiotemporal analysis of optical imaging data. Neuroimage 2003;18:610–621. [PubMed: 12667838]

Sornborger A, Yokoo T, Delorme A, Sailstad C, Sirovich L. Extraction of the average and differential dynamical response in stimulus-locked experimental data. J Neurosci Methods 2005;141:223–229. [PubMed: 15661304]

Stetter M, Schiessl I, Otto T, Sengpiel F, Hubener M, Bonhoeffer T, Obermayer K. Principal component analysis and blind separation of sources for optical imaging of intrinsic signals. Neuroimage 2000;11:482–490. [PubMed: 10806034]

Swindale NV. Orientation tuning curves: empirical description and estimation of parameters. Biol Cybern 1998;78:45–56. [PubMed: 9518026]

Swindale NV, Grinvald A, Shmuel A. The spatial pattern of response magnitude and selectivity for orientation and direction in cat visual cortex. Cereb Cortex 2003;13:225–238. [PubMed: 12571113]

Swindale NV, Matsubara JA, Cynader MS. Surface organization of orientation and direction selectivity in cat area 18. J Neurosci 1987;7:1414–1427. [PubMed: 3572486]

Tolhurst DJ, Dean AF, Thompson ID. Preferred direction of movement as an element in the organization of cat visual cortex. Exp Brain Res 1981;44:340–342. [PubMed: 7308348]

Vanni MP, Provost J, Lesage F, Casanova C. Evaluation of receptive field size from higher harmonics in visuotopic mapping using continuous stimulation optical imaging. J Neurosci Methods. submitted

Vanni MP, Villeneuve MY, Provost J, Lesage F, Casanova C. Orientation and direction selectivity in the cat visual cortex by spectral decomposition of the optical imaging signals. SfN abstract prog 2007:920.11.

Villeneuve MY, Vanni MP, Casanova C. Modular Organization in Area 21a of the Cat Revealed by Optical Imaging: Comparison with the Primary Visual Cortex. Neuroscience. submitted

Wagor E, Mangini NJ, Pearlman AL. Retinotopic organization of striate and extrastriate visual cortex in the mouse. J Comp Neurol 1980;193:187–202. [PubMed: 6776164]

Womelsdorf T, Eysel UT, Kisvarday ZF. Comparison of orientation maps obtained with different number of stimulus orientations. Neuroimage 2001;13:1131–1139. [PubMed: 11352618]

Worgotter F, Eysel UT. Quantitative determination of orientational and directional components in the response of visual cortical cells to moving stimuli. Biol Cybern 1987;57:349–355. [PubMed: 3435723]

Yokoo T, Knight BW, Sirovich L. An optimization approach to signal extraction from noisy multivariate data. Neuroimage 2001;14:1309–1326. [PubMed: 11707087]

Zepeda A, Arias C, Sengpiel F. Optical imaging of intrinsic signals: recent developments in the methodology and its applications. J Neurosci Methods 2004;136:1–21. [PubMed: 15126041]

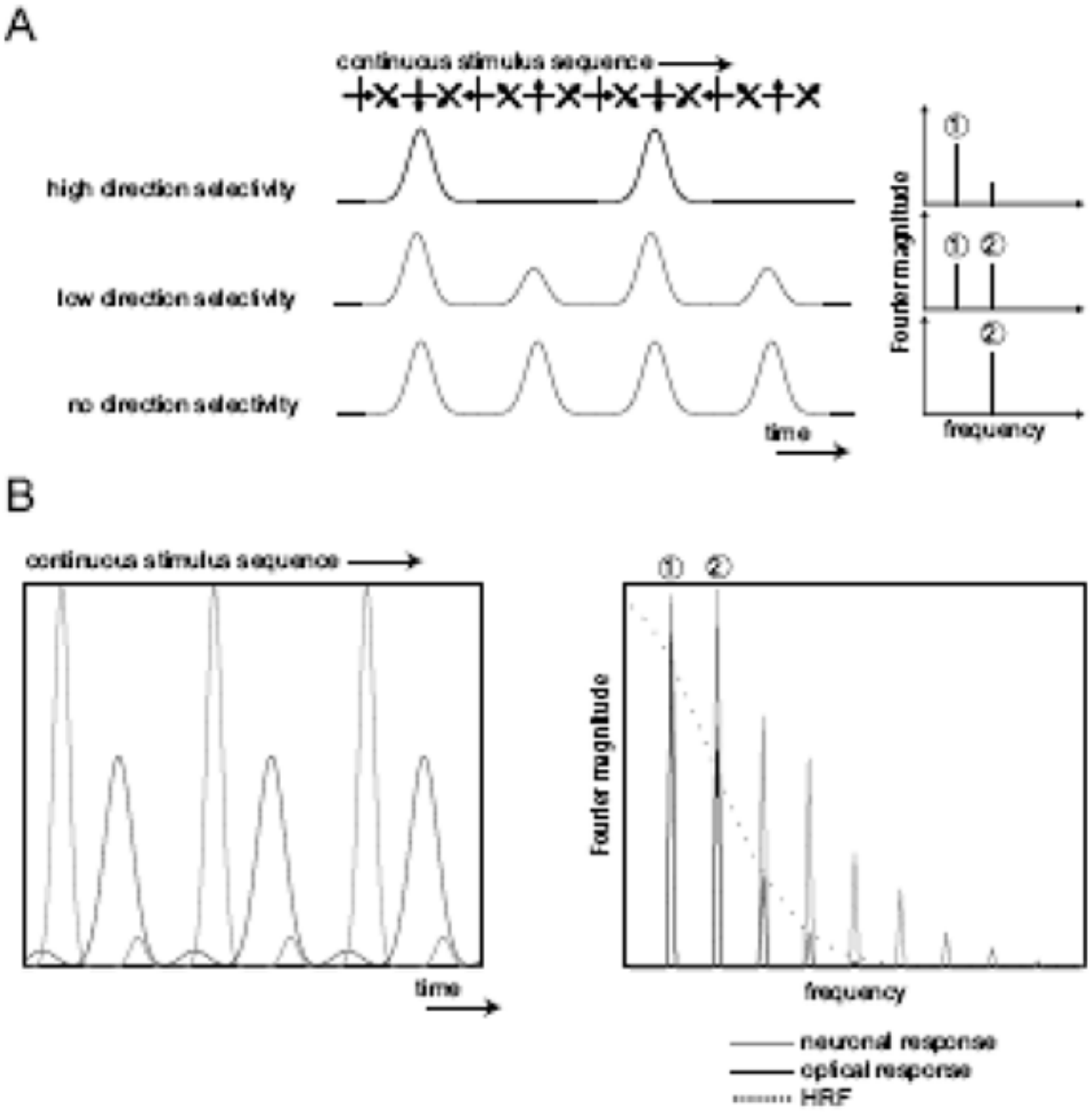

Figure 1.
(A). Diagram of the neuronal response and Fourier decomposition for three degrees of direction selectivity. (B). Schematic of the neuronal (gray) and optical (black) responses in temporal (left) and frequency (right) spaces.

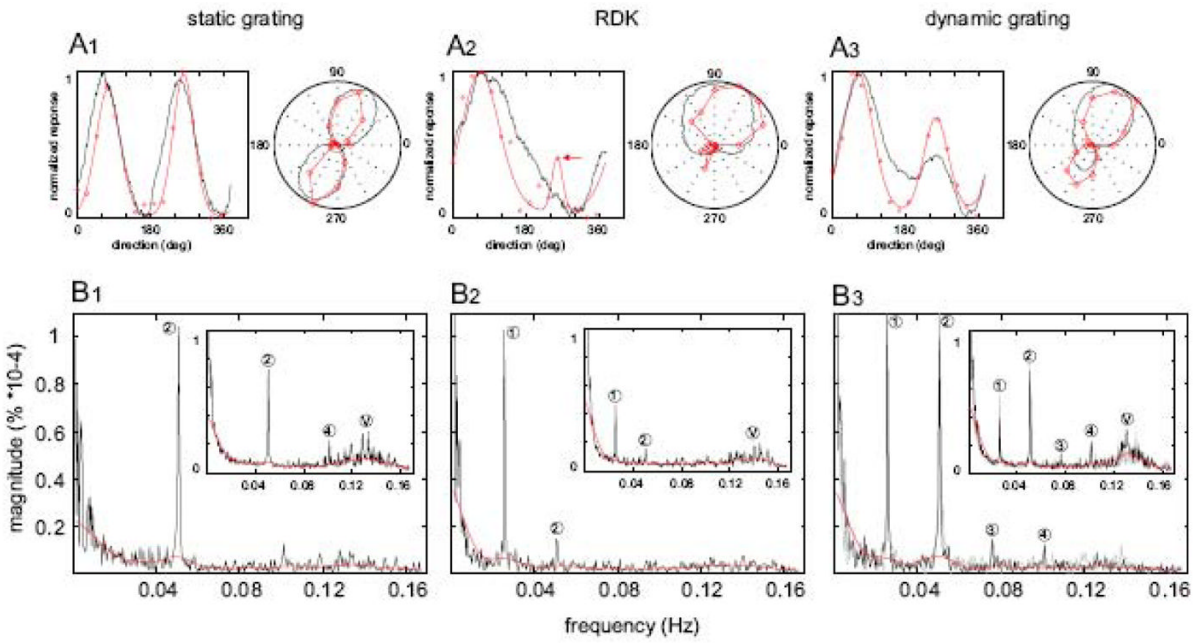

Figure 2.

(A) Profile of the response in one location of area 18 (indicated in Figure 3) with periodic (black) and episodic (red) paradigms for three stimuli: RDK, static and dynamic gratings. Red lines in the left tuning curves are the fit by the Von Mises function. In panel A2, the response to the opposite direction appearing at 247.5 deg was the result of noise contribution (filled arrow). (B) Fourier transform of the profiles with the periodic paradigm where first, second, third and fourth harmonics are indicated. Stimulus frequency (rotation) was 0.025 Hz (1/40s). Red lines are the baseline of the physiological noise and were used to correct the spectra for quantification. Inset: average spectra of every location indicated by the box in Figure 2. Abbreviation V: Vasomotion (and thereafter in Figures 6, 8 and 10). Gray spectra in B3 are obtained with a clockwise stimulation.

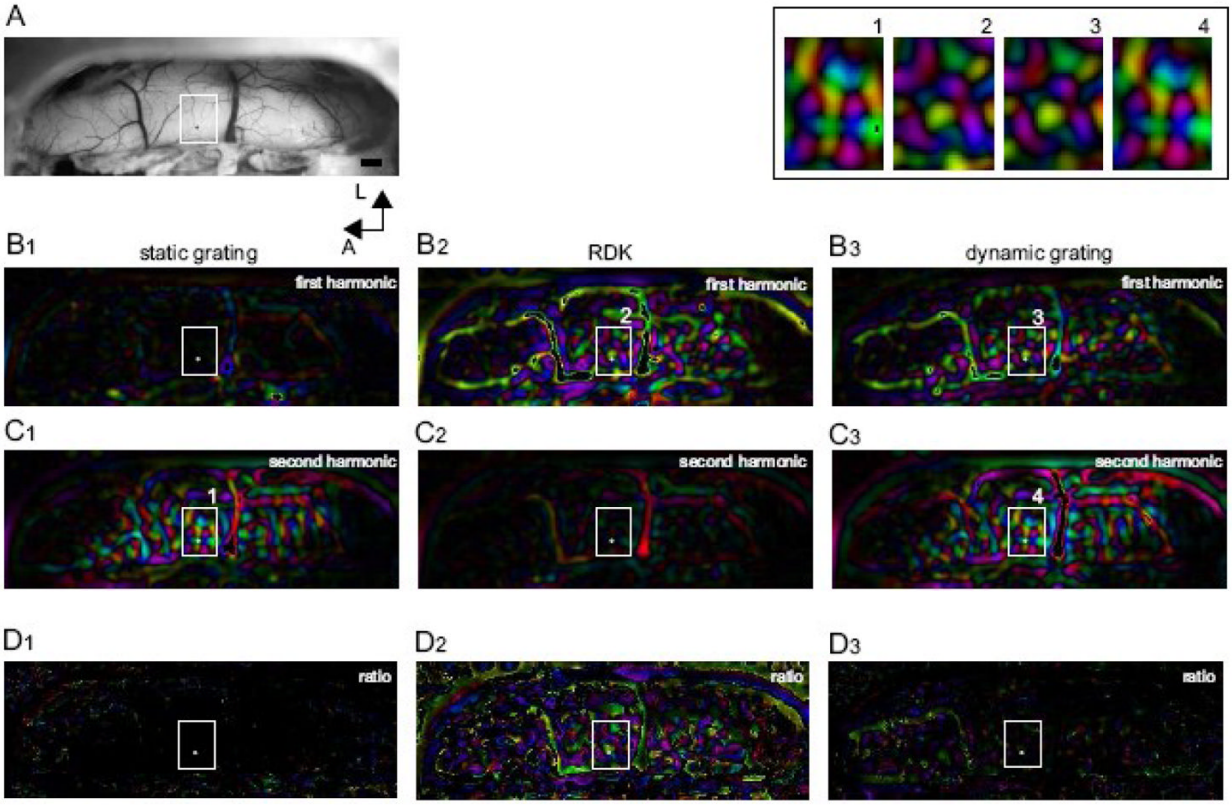

Figure 3.

(A) Vasculature pattern in the region of interest in area 18. The circle indicates the location of the pixel used in Figure 2. The box shows the location of the group of pixels used for quantification in Figures 2, 4, 5 and 6. Scale bar = 1mm. (B and C) Phase maps normalized by amplitude maps at the first and second harmonic for three stimuli: RDK, static and dynamic grating. (D) Phase maps at the first harmonic normalized by the ratio of the first to second harmonic (PDI′). Fourier phases have been corrected to facilitate the comparison with episodic paradigm in Figure 4. Boxes labelled 1 (in C1), 2 (B2), 3 (C3) and 4 (B3) were enlarged and shown in the upper-right inset.

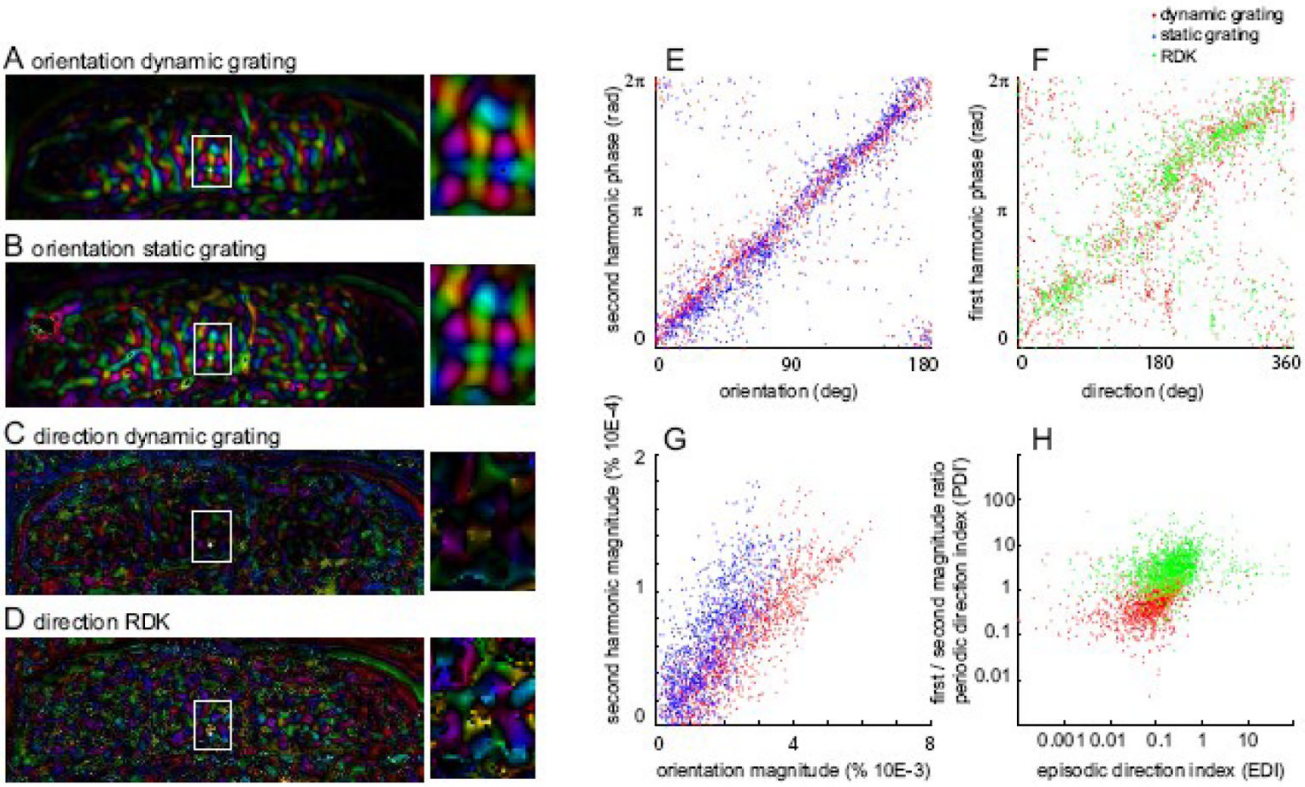

Figure 4.

Maps from episodic paradigm and Von Mises Fitting in the same region of interest as in Figure 3. (A and B) Preferred orientation normalized by the amplitude for dynamic and static gratings. (C and D) Preferred direction normalized by the direction index EDI for dynamic grating and RDK. (E) Phase at the second harmonic (Figure 3, panel C) as a function of the preferred orientation for static and dynamic gratings (panels A and B). (F) Phase at the first harmonic (Figure 3, panels B) as a function of the preferred direction for dynamic grating and RDK (panels C and D). (G) Amplitude at the second harmonic (Figure 3, panels C) as a function of the orientation amplitude for static and dynamic gratings (panels A and B). (H) PDI′s (Figure 3, panels D) as a function of the direction index (EDI) (panels C and D). Representation is in logarithmic scale.

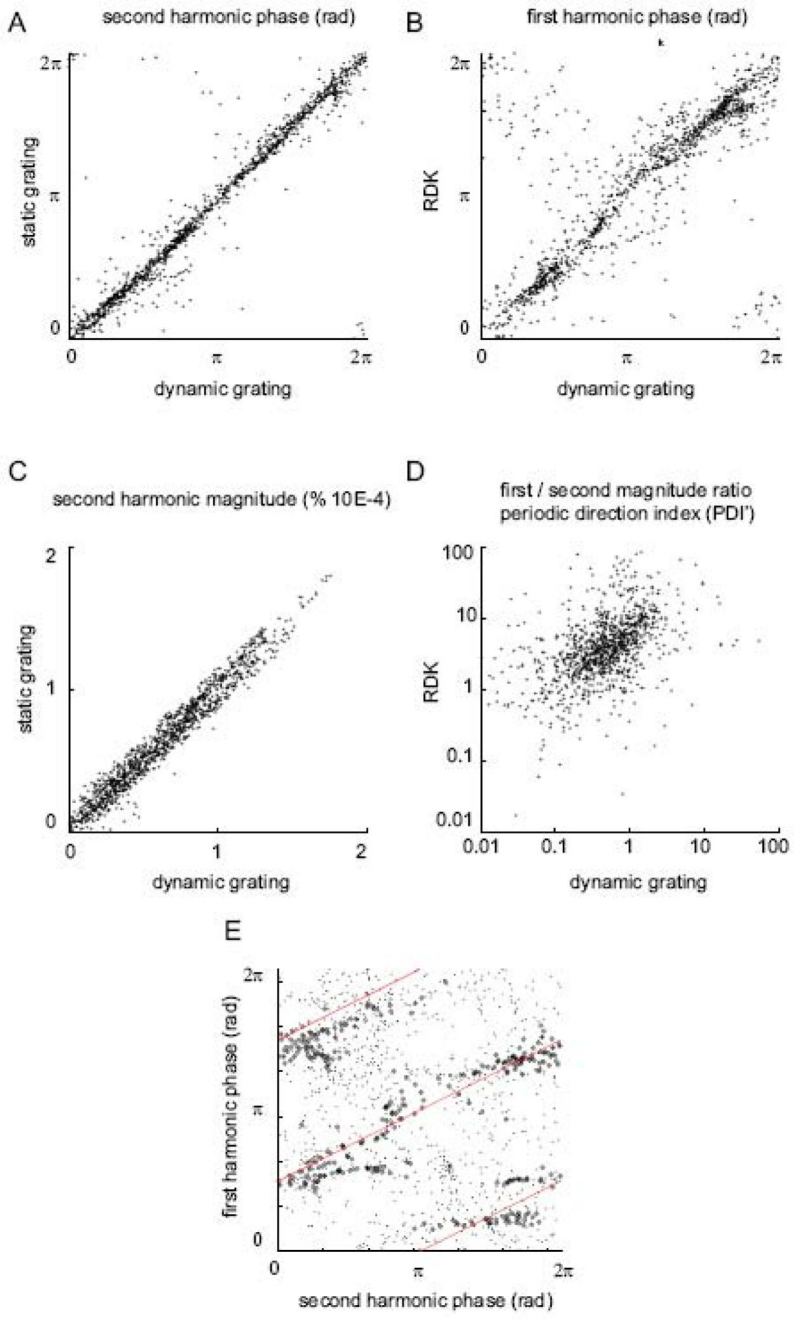

Figure 5.

Scatter plots illustrating the relationship between: (A) Second harmonic phases for static and dynamic gratings in a region of interest indicated by the white boxes in Figure 3. (B) First harmonic phases for dynamic grating and RDK. (C) Harmonic amplitudes for static and dynamic gratings. (D) PDI′s for dynamic grating and RDK. (E) First harmonic and second harmonic phases for dynamic grating, for all pixels (points) and pixels corresponding to high first harmonic amplitude and low phase gradient (circle, see method for gradient).

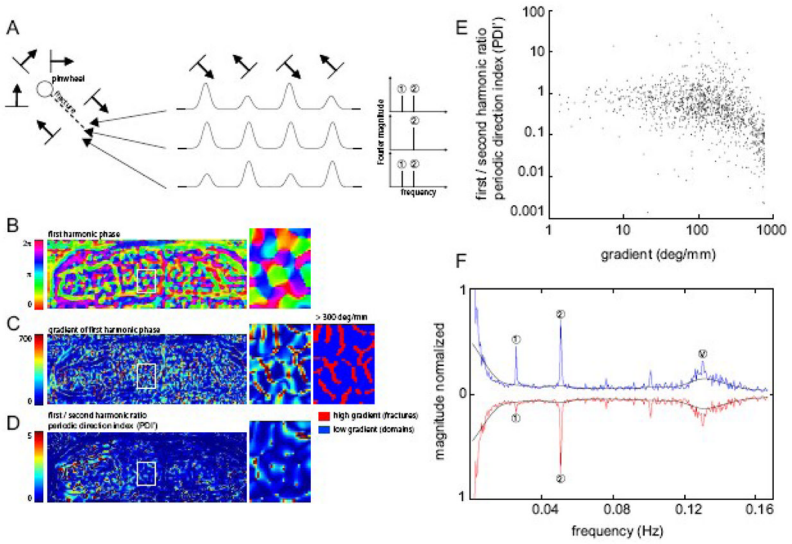

Figure 6.

A) Diagram of the estimated response profile in the direction map. Under fracture, the direction selectivity is reduced causing a decrease at the first harmonic. (B) Phase of the first harmonic for a dynamic grating (from panel B2 in Figure 3). (C) Gradient of the phase at the first harmonic. Note that the 2π range of phase was converted in 360 degrees of direction because gradient is a relative computation, unaffected by the non-correction of the hemodynamic delay. The second right magnification is the location of fracture (in red) and direction domains (in blue) with an arbitrary threshold of 300 deg/mm. (D) map of first/second harmonic ratio (PDI ′). (E) Scatter plot of the PDI′ as a function of the gradient in logarithmic scale. (F) Average spectra in pixels of fracture (red) and domains (blue) indicated in panel C.

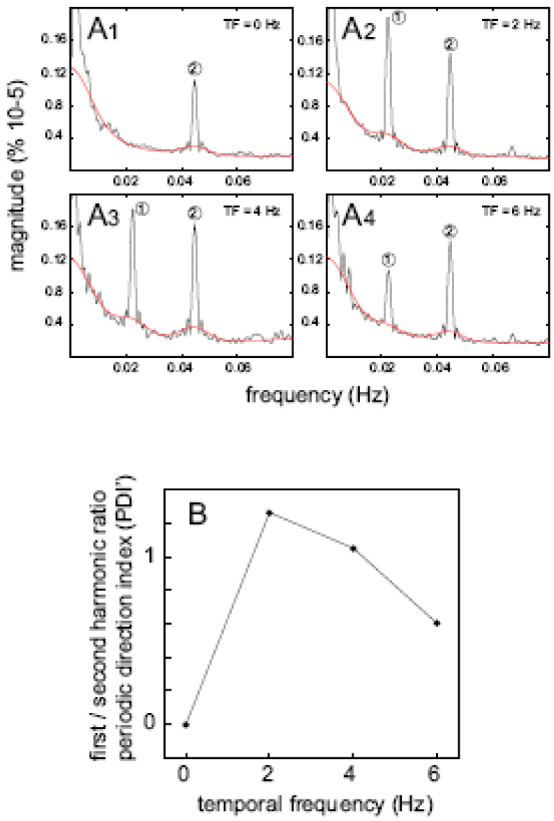

Figure 7.

(A) Spectra recorded in area 18 of case 2 for a grating drifting at four temporal frequencies: 0, 2, 4 and 6 Hz (velocities: 0, 13, 27 and 40 deg/s). Stimulus frequency (rotation) was 0.022 Hz (1/45s). (B) PDI′ measured from panel A as a function of temporal frequency.

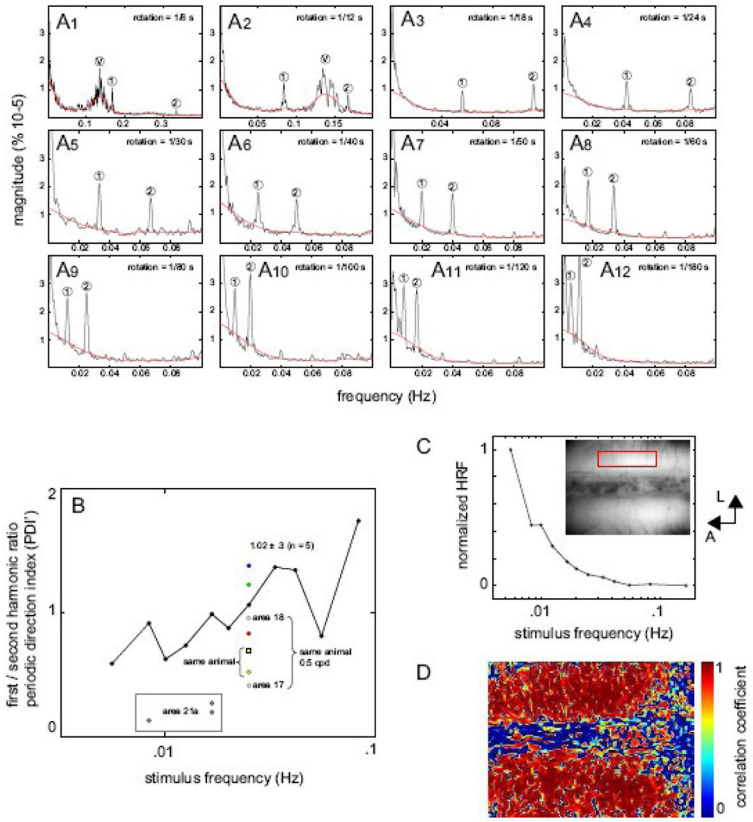

Figure 8.

(A) Spectra recorded for 12 stimulus frequencies (Hz): 0.167, 0.083, 0.056, 0.042, 0.033, 0.025, 0.020, 0.017, 0.012, 0.010, 0.008 and 0.006 (in sec: 1/6, 1/12, 1/18, 1/24, 1/30, 1/40, 1/50, 1/60, 1/80, 1/100, 1/120 and 1/180). (B) PDI′ measured from panels A as a function of the stimulus frequency (from case 2, in logarithmic scale). Coloured points (red, green and blue) indicate PDI′s measured in area 18 of cases 4 to 6 at the same stimulus frequency (0.025 Hz). Yellow points are the measurements for the dynamic grating shown in Figure 3 (case 1, circle: counter-clockwise stimulation, square: clockwise stimulation). The mean (±SD) is indicated in the Figure. Gray points are the measures in area 21a shown in Figure 9 (case 3, frequency = 0.008 and 0.017 Hz). White points are measures in area 17 and 18 shown in Figure 9 for a 0.5 c/deg dynamic grating (case 1). (C) Spectral distribution of the HRF obtained from the second harmonic signals (shown in panels A) in a ROI (red box in inset). (D) Correlation coefficients between the normalized HRF profile of each pixel and the reference profile shown in panel C.

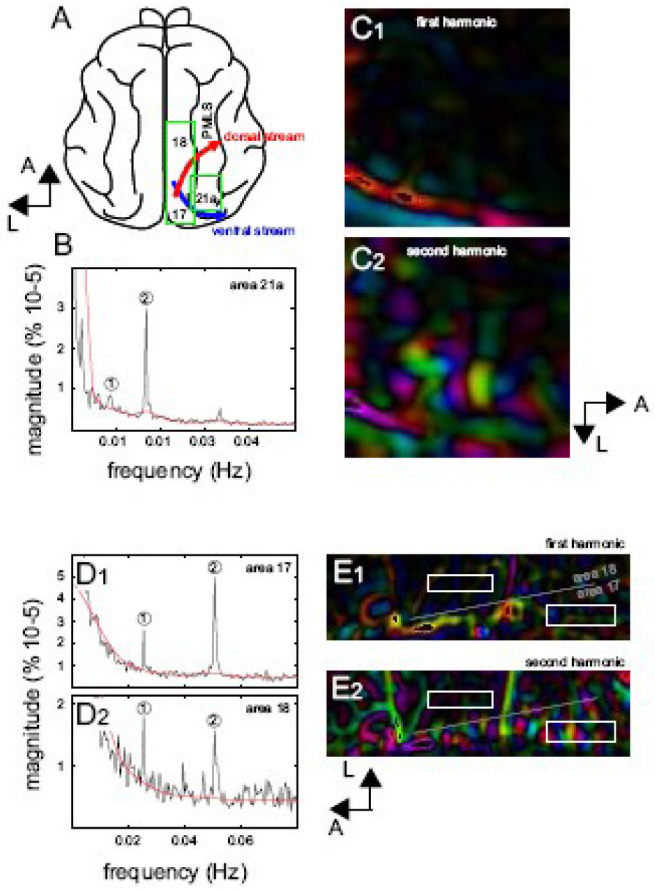

Figure 9.

(A) Diagram of the cat brain cortex where the ventral and dorsal streams are displayed, inspired from (Lomber, 2001). (B) Spectrum recorded in area 21a of case 3. (C) Phase map normalized by amplitude map at the first (C1) and second harmonic (C2). (D) Spectrum recorded in area 17 and 18 for a dynamic grating (0.5 c/deg, 3Hz). (E) Phase map normalized by amplitude map at the first (E1) and second harmonic (E2). ROI for quantification of the spectra in areas 17 and 18 are indicated by white boxes.

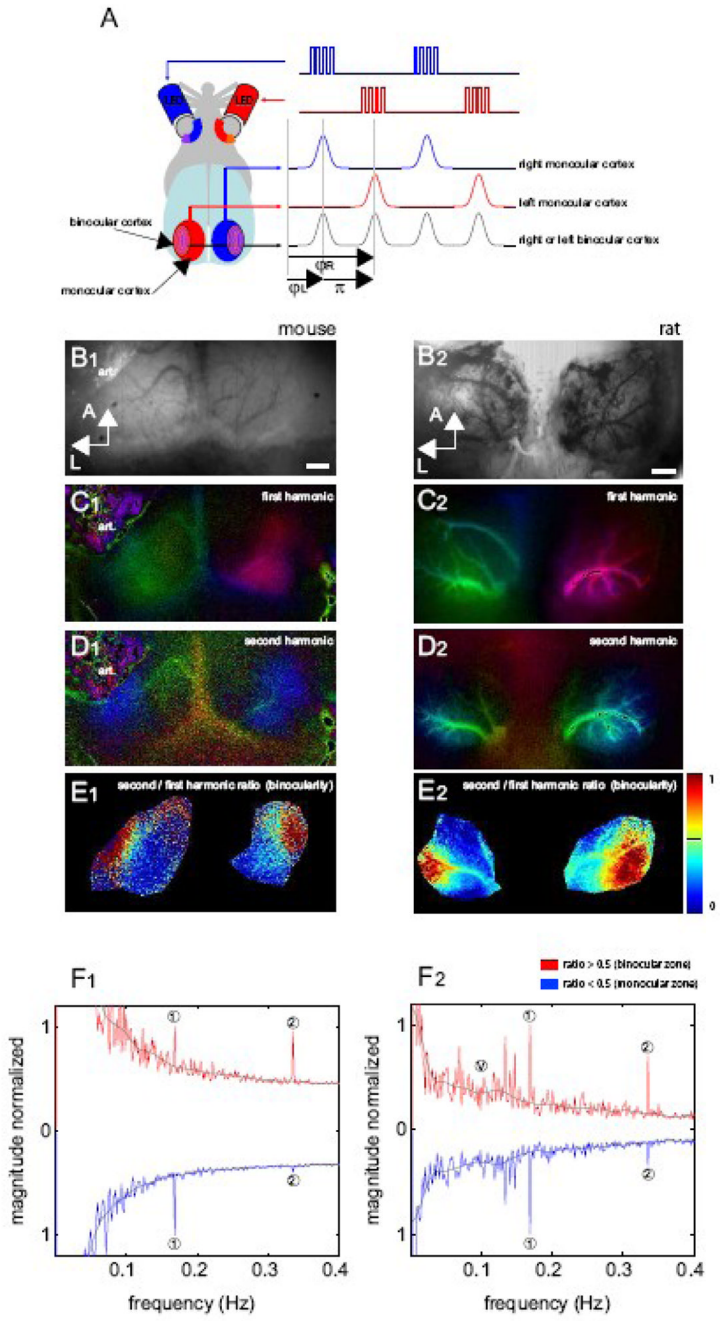

Figure 10.

(A) Diagram of the visual projections in rodents. Monocular visual cortex of each hemisphere receives information from the contralateral eye. Binocular visual cortex, lateral to the monocular parts, receive information from both eyes and are associated with a field of view in the front of the animal. White LED was fitted on the corneas and stimulated each eye in an alternate manner. Binocular regions are activated for each LED stimulation instead of monocular regions. (B) Vasculature pattern in the region of interest on the visual cortex of mouse (panels 1) and rat (panels 2). Scale bar = 1mm, Art.: artefact. (C and D) Phase map normalized by amplitude map at the first and the second harmonics. Stimulus frequency was 0.167 Hz (1/6s). (E) Ratio of the second/first harmonic maps. (F) Average spectra in pixels of

high ratio (> 0.5, in red) and low ratio (< 0.5, in blue) in a region of interest delimited in panel E.

Table 1

Correlation coefficients (r) between phase maps as a function of the time of recording. Numbers in brackets are the signal to noise ratio (SNR) defined as the peak amplitude to noise floor measure.

min vs. min	Second harmonic r (SNR)	First harmonic r (SNR)
15 vs. 15	0.91	0.83
30 vs. 15	0.97 (6.5)	0.88 (3.3)
30 vs. 10	0.98 (6.5)	0.88 (1.8)
30 vs. 5	0.96 (5.0)	0.72 (0.7)
30 vs. 3	0.96 (3.3)	0.63 (0.6)
30 vs. 2	0.94 (2.4)	0.69 (0.7)
30 vs. 1	0.87 (2.1)	0.47 (0.6)

Table 2

Correlation coefficients (r) between phase maps as a function of the temporal frequency.

	0 vs 2 Hz	**0 vs 4 Hz**	**0 vs 6 Hz**	**2 vs 4 Hz**	**4 vs 6 Hz**	**2 vs 6 Hz**
Orientation (2nd harmonic)	0.81	0.74	0.77	0.92	0.89	0.91
Direction (1st harmonic)	−0.07	−0.07	0.05	0.87	0.78	0.72